STATIONARY AND TIME-DEPENDENT MHD SIMULATIONS OF THE SOLAR WIND

R. Keppens, J.P. Goedbloed

FOM-Institute for Plasma Physics 'Rijnhuizen', P.O. Box 1207, 3430 BE Nieuwegein, The Netherlands
keppens@rijnh.nl goedbloed@rijnh.nl

ABSTRACT

We initiated a gradual approach towards dynamic solar/stellar wind numerical simulations in three dimensions with the equations of magnetohydrodynamics. In a recent publication (Keppens & Goedbloed 1999, Astron. Astrophys. 343, 251), we proceeded stepwise from a spherically symmetric, isothermal, unmagnetized, non-rotating Parker wind to arrive at axisymmetric, polytropic, magnetized, rotating models. These 2D generalisations of the analytical Weber-Davis wind solution, can contain both a 'wind' and a 'dead' zone. For these axisymmetric, steady-state solutions, we use the knowledge of the flux functions to verify the physical correctness of the numerical solutions.

Since then, we studied the influence of the magnetic field strength and topology by varying the extent of the dead zone, of the stellar rotation, and of sudden mass ejecta on axisymmetric MHD winds (Keppens & Goedbloed 1999, Astrophys. J., submitted). Reasonable changes in the coronal magnetic field – factor of two – alter the detailed acceleration behaviour of the wind. Larger dead zones cause effective, fairly isotropic acceleration to super-Alfvénic velocities as the polar, open field lines are forced to fan out rapidly with radial distance. In the ecliptic, the wind outflow is modulated by the extent of the dead zone. Coronal mass ejections are simulated on top of these transonic outflows.

Key words: MHD — solar wind — Methods: numerical

1. INTRODUCTION

We continue our gradual approach towards dynamic solar wind simulations in 3D MHD. In Keppens & Goedbloed (1999a), we systematically generalized the well-known Parker (1958) and magnetized Weber & Davis (1967) wind models out of the equatorial plane to yield polytropic, axisymmetric and transonic outflow from magnetized, rotating stars. An example for a split-monopole base field and a solar rotation rate of $\Omega_\odot = 2.998 \times 10^{-6}\,\mathrm{s}^{-1}$ is shown in Fig. 1. The solution has a coronal base field of about 2 G, a base temperature of 1.5×10^6 K, with a number density of $10^8\,\mathrm{cm}^{-3}$. This type of field was also used by Sakurai (1985) and the resulting wind solution defines the critical surfaces, through which the outflow accelerates continuously from subslow flow at the surface to superfast flow at large distances.

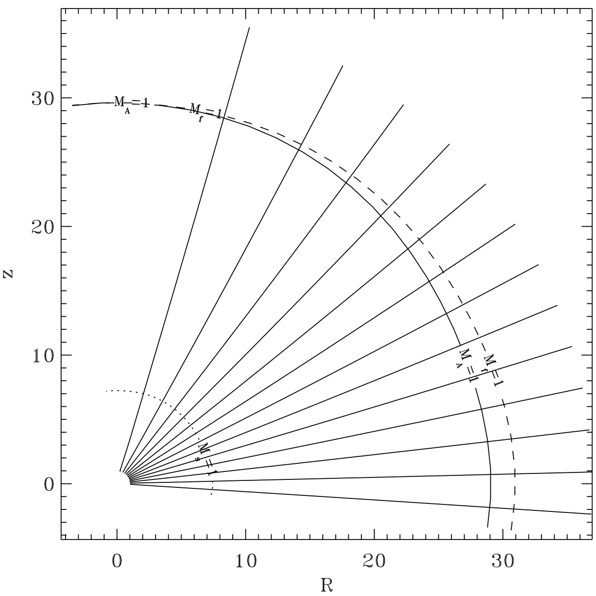

Figure 1. As in Keppens & Goedbloed (1999a): an axisymmetric MHD wind from the rotating sun. The base field is a split-monopole. We show streamlines and the positions of the critical surfaces.

The poloidal streamlines and poloidal field lines, with constant $\psi(R,Z)$, are parallel. We use cylindrical coordinates (R, Z, φ). In ideal MHD, one obtains various flux functions conserved along the streamlines, like $\Lambda(\psi) = Rv_\varphi - RB_\varphi B_p/\rho v_p$, where ρ is the density and B_p (v_p) indicates the poloidal magnetic field (velocity). The polytropic condition implies that the entropy is constant $S = 1/\gamma$, with γ the polytropic index. We took $\gamma = 1.13$. We verify $\Omega(\psi) = \left[v_\varphi - (v_p/B_p)B_\varphi\right]/R$ and the Bernoulli function $H(\psi) = \left[v_R^2 + v_Z^2 + v_\varphi^2\right]/2 + \rho^{\gamma-1}\gamma S/(\gamma-1) - GM_\odot/r - R\Omega v_\varphi$.

2. WINDS CONTAINING A 'DEAD' ZONE

If we initialize the time-marching procedure to obtain steady-state stellar wind solutions with a mixed monopolar wind and dipolar dead zone, we find magnetized, rotating winds containing helmet streamers. An example solution is in Fig. 2. The polytropic solutions generalize the isothermal model by Pneuman & Kopp (1971) of a mixed open-closed magnetic wind structure by including the effects of rotation. The stellar rotation causes a toroidal winding of the field lines and the resulting azimuthal field component B_φ is shown in gray-scale in the figure. It was pointed out by Suess & Nerney (1973) how this ultimately leads to a poleward collimation of the field due to an asymptotic meridional flow pattern $v_\theta \propto -\sin(2\theta)$. The solutions agree with this predicted pole-to-pole variation of v_θ at large radial distances, as demonstrated in Keppens & Goedbloed (1999b).

Boundary conditions at the stellar surface impose the mass flux and ensure the correct rotational coupling of velocity and magnetic field by prescribing the flux function Ω at the base. We let the density and all magnetic field components adjust freely there. When we take a latitudinally dependent mass flux, we model the closed field line regions self-consistently as dead zones from which no plasma escapes. Note the way in which the outflow accelerates to superfast flow. This is characterized by the critical surfaces where the poloidal flow exceeds the poloidal slow, Alfvén, and fast velocities.

The resulting – calculated – base number density varies as shown in Fig. 3, with a clear imprint of the dead zone. The figure also contains number density cuts at larger fixed radial distances, not intersecting the dead zone. The higher densities about the equator are consistent with the observations. In Fig. 4, we show the obtained number density decrease above the poles. A recent determination of the variation of the electron density with height above a polar coronal hole by Doyle et al. (1999) quoted the dependencies $N_e(r) \propto r^{-8}$ within 1–2 $R_\odot$, $N(r) \propto r^{-4}$ within 2–4 $R_\odot$, and a r^{-2} variation further out. We overplotted these observed variations in the figure. While the base density variation is not quite as steep as observed, a clear trend in slope is visible with a remarkable agreement around 3 $R_\odot$.

3. VARYING THE CORONAL B FIELD

In Keppens & Goedbloed (1999b), we investigate how reasonable changes in the coronal magnetic field alter the detailed acceleration behaviour of the wind. Since we control the extent of the resulting dead zone through the base radial mass flux, we can explore the effects of its size and separate it from the effects in coronal magnetic field strength. We compared the solution shown in Fig. 2 with (i) one with a dead zone twice as large; (ii) one with a base field twice as strong; and (iii) one where both field strength and dead zone extent were doubled. The changes in the gobal wind pattern were qualified by the resulting deformations of the critical surfaces. We quantified their effect on the polar and equatorial poloidal speed

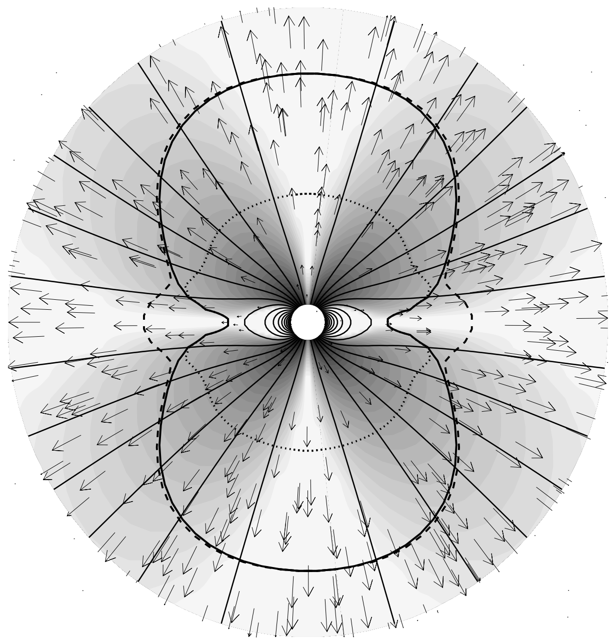

Figure 2. As in Keppens & Goedbloed (1999b): for the same solar-like conditions as in Fig. 1, a magnetized, rotating wind with an equatorial dead zone. Critical slow, Alfvén and fast curves are indicated, with the helmet-streamer cusp coinciding with the Alfvénic transition (solid hourglass curve) on the equator. The rotation causes the gray-scale $\mid B_\varphi \mid$ variation. With the bottom boundary at $1.25 R_\odot$, the plotted region stretches out to $22.5 R_\odot$.

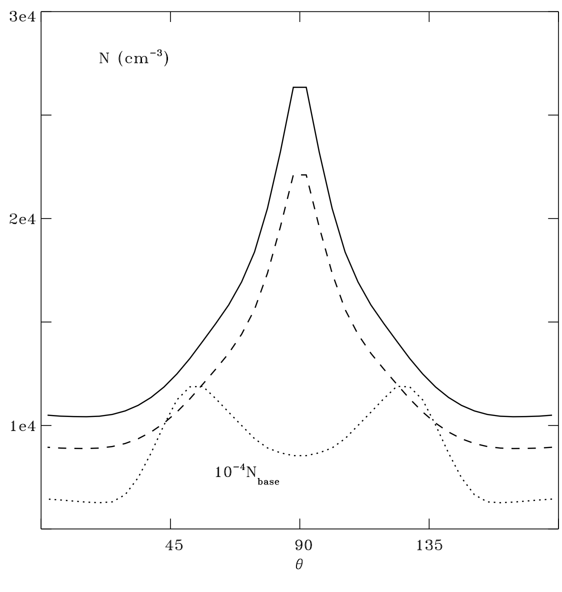

Figure 3. The number density as a function of polar angle at $11.9 R_\odot$ (solid), $12.7 R_\odot$ (dashed), and at the base $1.27 R_\odot$ (dotted and scaled to fit on the figure).

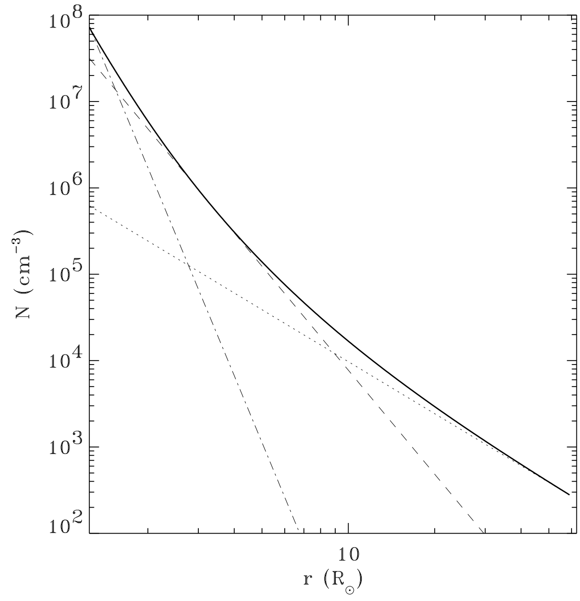

Figure 4. The number density above the poles as a function of radius for the MHD model from Fig. 2. In this log-log plot, the straight lines indicate observed variations going like r^{-8} (dash-dotted), r^{-4} (dashed), and r^{-2} (dotted).

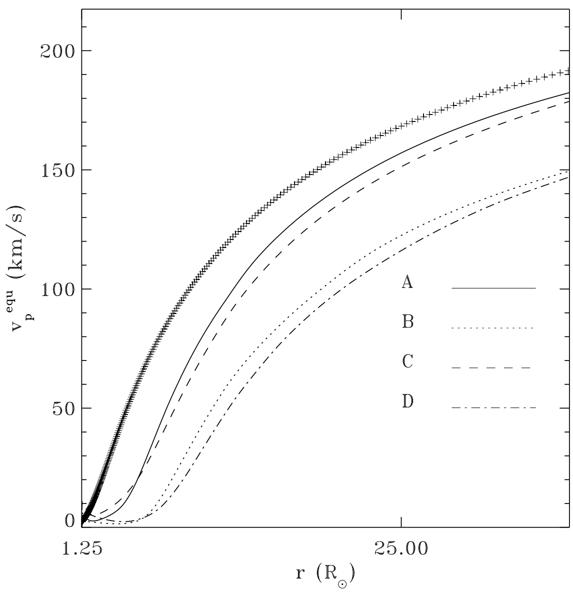

Figure 5. The equatorial poloidal velocity from five different models: split-monopole with 2 G **B** field (crosses); (A) small dead zone; (B) large dead zone; (C) small dead zone, 4 G field; (D) large dead zone with 4 G field.

and on the equatorial toroidal velocity. The equatorial poloidal velocities as a function of radius for five different wind solutions are compared in Fig. 5. The five models are

- the 'split-monopole' one shown in Fig. 1 which has a ~ 2 G base field;
- the corresponding wind solution with a $\pm 30°$ equatorial dead zone shown in Fig. 2;
- a solution with a $\pm 60°$ dead zone;
- a solution with a $\simeq 4$ G base field and $\pm 30°$ dead zone;
- one with a $\pm 60°$ dead zone and a $\simeq 4$ G base field.

Note that the presence of the dead zone reduces the equatorial velocities by 10 to 40 km/s depending on its size and base field strength.

It was found that the larger dead zone forces the open field lines to fan out rapidly. The plasma gets accelerated more efficiently closer to the stellar surface. A stronger field renders the critical curves more anisotropic, as the polar slow transition shifts inwards and the Alfvén and fast outwards. Doubling both, these effects interplay such that the spin-down torque exerted by the wind on the star remains approximately constant.

Under the chosen parameter values, all these wind solutions are still thermally driven and mimick solar conditions. Similar changes of only a factor of two in field strength and topology could occur in the solar wind pattern within its 11-year magnetic cycle.

4. TIME-DEPENDENT PHENOMENA

CMEs represent major disturbances on top of the stationary transonic solar wind. Although they are associated with sudden, significant mass loss and violent disruptions of the global field pattern, one frequently observes the global coronal wind structure to return to its previous stationary state. Since we impose the base mass flux, we can trigger CMEs on top of the outflow pattern and study their motion out to large radial distances. At the same time, we can demonstrate that the numerical solutions are stable to such violent perturbations by returning to a largely unchanged stationary state. In Keppens & Goedbloed (1999b), we showed how the overall wind pattern reacts to a localized, short-lived, large-amplitude mass flux increase. Figure 6 shows how a mass ejection involving roughly 10^{17} g of solar plasma influences the meridional field configuration. The times indicated are measured from the onset: the modeled CME detaches from the base within 45 minutes. A hypothetical spacecraft at $26R_\odot$, close to the ecliptic, would record the CME-passage as a sudden increase in density and poloidal velocity which eventually relax to their pre-event levels. The event is followed by an increased azimuthal flow regime and shows large oscillations in **B** strength and orientation.

5. DISCUSSION AND CONCLUSIONS

In a sequence of stationary, 1D, 1.5D, and 2.5D, hydrodynamic and magnetohydrodynamic stellar wind models, all obtained with the Versatile Advection Code – see Tóth (1996) and

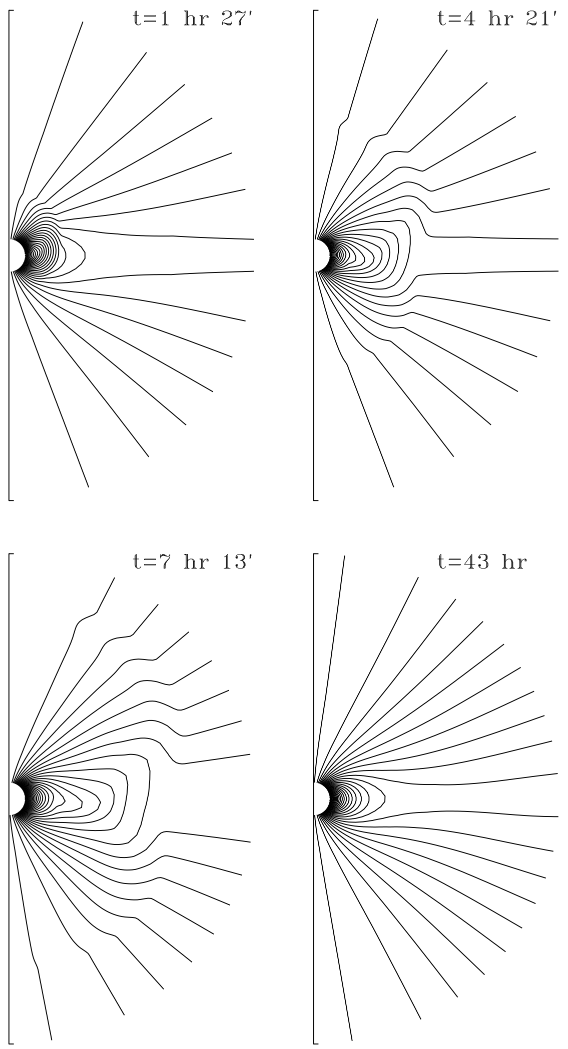

Figure 6. A violent coronal mass ejection distorts the field structure throughout the poloidal plane (first three times shown), but the overall wind pattern returns to a stationary transonic flow with mixed open-closed field lines after its passage. The plotted region covers the first $19R_{\odot}$.

`http://www.phys.uu.nl/~toth` – we demonstrated how we can now routinely calculate axisymmetric magnetized wind solutions for (differentially) rotating stars. The field topology can have both open and closed field line regions, so that we model 'wind' and 'dead' zones self-consistently.

Such models show evidence for a transition from high density, low speed equatorial wind to lower density, high speed polar wind. The density fall-off with height at the poles agrees well with the observed variation. Changes in the coronal field strength and topology have a clear impact on the wind pattern: a faster polar acceleration can result from modest increases in **B** strength and dead zone extent. The axisymmetric models presented here are stable to violent mass dumps, but it remains to be shown how truly 3D perturbations evolve on top of magnetized transonic flows.

For the stationary, axisymmetric MHD solutions, the analytic framework used to classify stationary MHD equilibria exhibiting a translational symmetry by Goedbloed & Lifschitz (1997) will be generalized to allow for axisymmetry. We recall that in the translationally symmetric case, ideal MHD flow regimes containing limiting line and Alfvén singularities must necessarily be connected across them by the three types of MHD shocks. In the axisymmetric wind solutions discussed here, a continuous acceleration through the critical surfaces is obtained instead: a paradox that needs to be resolved.

In future work, specific interest will be given to details in the wind structure, e.g. the boundaries of open and closed field line regions or the heliospheric current sheet. Recent progress made by numerically simulating multi-dimensional, magnetized shear layers in Keppens et al. (1999) and Keppens & Tóth (1999) will aid in the systematic study of the plasma dynamics at those locations. With the non-linear interactions of Kelvin-Helmholtz and resistive instabilities understood in idealized settings (2D current-vortex sheets and 3D magnetized jets), the ultimate goal is to reach a synergy of these results where global solar wind models consist of stationary wind patterns containing dynamic current-vortex sheet regions.

Acknowledgements. This work was performed as part of the research programme of FOM, in the NWO project on 'Parallel Computational Magneto-Fluid Dynamics'. It was sponsored by NCF for use of supercomputer facilities.

REFERENCES

Doyle, J.G., Teriaca, L., Banerjee, D., Fludra, A., & Keenan, F.P. 1999, Proceedings of '8th SOHO workshop', 22–25 June, Paris, France. To appear in ESA SP-446.

Goedbloed, J.P., & Lifschitz, A. 1997, Phys. of Plasmas 4 (10), 3544

Keppens, R., & Goedbloed, J. P. 1999a, Astron. Astrophys. 343, 251

Keppens, R., & Goedbloed, J. P. 1999b, Astrophys. J., submitted

Keppens, R., Tóth, G., Westermann, R. H. J., & Goedbloed, J. P. 1999, J. Plasma Phys. 61 (1), 1

Keppens, R., & Tóth, G. 1999, Phys. of Plasmas 6 (5), 1461

Parker, E.N. 1958, Astrophys. J. 128, 664

Pneuman, G.W., & Kopp, R.A. 1971, Sol. Phys. 18, 258

Sakurai, T., 1985, Astron. Astrophys. 152, 121

Suess, S.T., & Nerney, S.F. 1973, Astrophys. J. 184, 17

Tóth, G. 1996, Astrophys. Lett. & Comm. 34, 245

Weber, E.J., & Davis, L. 1967, Astrophys. J. 148, 217